Ultra-wideband and broad-angle linear polarization conversion metasurface

Hengyi Sun, Changqing Gu, Xinlei Chen, Zhuo Li, Liangliang Liu, and Ferran Martín

Citation: Journal of Applied Physics **121**, 174902 (2017); doi: 10.1063/1.4982916
View online: http://dx.doi.org/10.1063/1.4982916
View Table of Contents: http://aip.scitation.org/toc/jap/121/17
Published by the American Institute of Physics

Ultra-wideband and broad-angle linear polarization conversion metasurface

Hengyi Sun,[1] Changqing Gu,[1,a)] Xinlei Chen,[1] Zhuo Li,[1,2] Liangliang Liu,[1] and Ferran Martín[3]

[1]*Key Laboratory of Radar Imaging and Microwave Photonics, Ministry of Education, College of Electronic and Information Engineering, Nanjing University of Aeronautics and Astronautics, Nanjing 210016, China*
[2]*State Key Laboratory of Millimeter Waves, Southeast University, Nanjing 210096, China*
[3]*CIMITEC, Departament d'Enginyeria Electrònica, Universitat Autònoma de Barcelona, Bellaterra, 08193 Barcelona, Spain*

(Received 13 February 2017; accepted 21 April 2017; published online 5 May 2017)

In this work, a metasurface acting as a linear polarization rotator, that can efficiently convert linearly polarized electromagnetic waves to cross polarized waves within an ultra wide frequency band and with a broad incident angle, is proposed. Based on the electric and magnetic resonant features of the unit cell, composed by a double-head arrow, a cut-wire, and two short V-shaped wire structures, three resonances, which lead to the bandwidth expansion of cross-polarization reflections, are generated. The simulation results show that an average polarization conversion ratio of 90% from 17.3 GHz to 42.2 GHz can be achieved. Furthermore, the designed metasurface exhibits its polarization insensitivity within a broad incident angle, from 0° to 50°. The experiments conducted on the fabricated metasurface are in good agreement with the simulations. The proposed metasurface can find potential applications in reflector antennas, imaging systems, and remote sensors operating at microwave frequencies. *Published by AIP Publishing.*
[http://dx.doi.org/10.1063/1.4982916]

I. INTRODUCTION

Metamaterials have enabled the realization of many fascinating phenomena and functionalities that cannot be obtained through the use of natural materials.[1,2] In recent years, the ability to fully manipulate the polarization states of electromagnetic (EM) waves allows us to envision potential applications which may greatly influence our daily lives in many consumer products and high-tech applications.[3,4] Concerning polarization converters, these devices are usually designed using twisted nematic liquid crystals based on the Faraday effect.[5] These traditional approaches and materials for polarization control are now being gradually replaced by the so-called metasurfaces, which have been intensively investigated in the past decade. Metasurfaces typically utilize asymmetric electric dipole resonances to allow 0 to 2π phase control of the cross-polarized scattered light. As in transmit arrays, varying the geometry of the resonator as a function of position allows for arbitrary control of the phase front of light using a subwavelength-thin film and has led to demonstrations including anomalous reflection/refraction,[6–10] polarization beam splitting,[11] polarization rotation,[12–16] and surface wave conversion.[17] Currently, anisotropic metamaterials have been widely applied in miniaturized polarization controllers.[18–20] However, these polarization devices have the disadvantage of narrow bandwidth, so that bandwidth expansion is one of the main research interests and challenges.

To broaden polarization conversion bandwidth, stacked multilayer structures can be used. As an example, a high-efficiency broadband polarization transformation slab was achieved by stacking twisted complementary circular symmetric split-ring resonators.[21] Gansel *et al.* proposed three-dimensional gold helices which can be scaled to microwave and terahertz frequencies and can be used as compact broadband circular polarizers.[22] Although these proposed polarization devices exhibit a relatively wide operating frequency band, complicated structures or unacceptable thicknesses may limit their practical applications. Hao *et al.* demonstrated that polarization states of electromagnetic waves can be manipulated through reflections by an anisotropic metamaterial plate by adjusting material parameters, and demonstrators at microwave and optical frequencies were reported.[23,24] Yu *et al.* designed a metasurface by using an V-shaped antenna array and verified numerically and experimentally that by changing the dimension and geometry of the V-shaped antenna, EM waves could be manipulated, including both phase and polarization.[25] Based on this method, Chen *et al.* proposed a double-head arrow structure[26] and Gao *et al.* proposed a double V-shaped structure,[27] to achieve ultra-wideband linear polarization conversion in the microwave regime.

In this paper, we propose an ultra-wideband linear polarization rotator by combining three typical symmetry-broken structures, i.e., a double-head arrow, a cut-wire, and two short V-shaped wire resonators. We show that the structure is able to rotate a linearly polarized wave into its orthogonal one. Through the generation of three resonances, we can expand the bandwidth of the cross-polarization reflection of the metasurface. Both numerical simulations and experimental results demonstrate that the polarization converter can change both *x*- and *y*-polarized waves into its cross-polarized waves under normal incidence. The rotating frequency range covers from 17.3 GHz to 42.2 GHz with efficiency near to

a)Electronic mail: gucq@nuaa.edu.cn

100% at the three resonance frequencies. In addition, the polarization conversion functionality is preserved under oblique incidence. Compared to other kinds of polarization devices, the proposed polarization converter is much thinner and covers a wider frequency range.

II. THEORY

It is known that reflection polarization conversion metasurfaces are usually implemented by multilayers with an artificial periodic metallic structure on the top, a metallic sheet layer at the bottom, and an intermediate dielectric in between. The periodic array is homogeneous and anisotropic, with dispersive relative permittivity and permeability. When a plane wave (PW) with a specified polarization impinges on this artificial electromagnetic metasurface, both *x*- and *y*-polarized EM waves can be generated by reflection and transmission due to the anisotropic characteristics of the metasurface. The waves experience multiple reflections between the artificial metallic structure and the metallic sheet layer, and the final reflected waves are a result of an interfering wave phenomenon. Thus, we can utilize the thickness of the dielectric layer to control the phase and amplitude of the final reflected waves.[28–31] Based on the operational principles described above, we selected the F4B dielectric spacer with the thickness $d = 1.5$ mm, dielectric constant $\varepsilon_r = 2.65$, and loss tangent $\tan\delta = 0.001$ (specifically, d has been optimized with the help of the commercial software simulator in order to achieve good polarization conversion, as will be shown later). The geometrical parameters of the metasurface unit cell are [see Fig. 1(a)]: $a = 3$ mm, $b = 1.5$ mm, $c = 0.45$ mm, $h = 0.6$ mm, $w = 0.2$ mm, $l = 2.6$ mm, $\alpha = 80°$, and $\beta = 90°$. The thickness of metallic patterns is 0.035 mm.

To better understand the response of the proposed structure, we consider that the incident EM wave is polarized along the *y*-axis. Therefore, the electric field can be decomposed into two perpendicular components (directions *u* and *v*, see Fig. 1(b)). Hence, the electric field of the incident EM wave can be expressed as

$$\vec{E} = \vec{u}E_{iu}e^{j\varphi} + \vec{v}E_{iv}e^{j\varphi}, \tag{1}$$

whereas the electric field of the reflected wave can be written as

$$\vec{E}_r = \tilde{r}_u\vec{u}E_{iu}e^{j\varphi} + \tilde{r}_v\vec{v}E_{iv}e^{j\varphi}, \tag{2}$$

where $\tilde{r}_u$ and $\tilde{r}_v$ are the reflection coefficients along the *u*- and *v*-axes, respectively.[27] Due to the anisotropic characteristic of the metasurface, a different phase change $\Delta\varphi$ can be generated by $\tilde{r}_u$ and $\tilde{r}_v$. Therefore, when $\Delta\varphi = \pi$ and the modulus satisfy $r_u = r_v$, then E_{ru} and E_{rv} will be the synthetic fields along with the *x*-direction, as shown in Fig. 1(b), and the incident polarization is rotated by 90°. In fact, the individual double-head arrow structure supports symmetric and anti-symmetric modes, which are excited by electric field components along the *v*- and *u*-axes, and the individual cut-wire structure supports multi-order dipolar resonances which are excited by electric field components along the *v*-axis. As for the combined structure, we predict the presence of multiple resonances. In order to validate this, we have simulated the reflection amplitude and phase of the unit cell in *CST Microwave Studio*. Figures 2(a) and 2(b) show that two eigen-modes are excited in the *v*-polarized case and one eigen-mode is excited in the *u*-polarized case. When arbitrarily polarized EM waves are incident, three resonances can be excited in general since both *v*- and *u*-components exist simultaneously. The superposed contributions from two individual orthogonal electric components excite independently the corresponding resonance eigen-modes.

Fig. 3 shows that the reflection amplitude of the polarization along the *v*-axis direction is approximately equal to the polarization along the *u*-axis. Moreover, the reflection phases approach π from 17.3 GHz to 42.2 GHz. It is evident that the metasurface can realize polarization conversion in a wide frequency range of 24.9 GHz. To further measure the performance of the polarization conversion of the designed artificial electromagnetic structure, we define the polarization conversion ratio (PCR) as

$$PCR = r_{xy}^2/(r_{xy}^2 + r_{yy}^2) = r_{yx}^2/(r_{yx}^2 + r_{xx}^2), \tag{3}$$

where r_{xx} and r_{yy} represent the co-polarization reflection coefficients and r_{yx} and r_{xy} represent the cross-polarization reflection coefficients, respectively. If PCR = 1, the complete transformation of both linear *x*- and *y*-polarized EM waves into each other is realized.

To investigate the physical mechanism of the ultra-wideband polarization conversion with the use of the proposed metasurface, the surface current distributions on the artificial electromagnetic structure and metallic ground sheet at three resonant frequencies of 16.38 GHz, 29.57 GHz, and 42.03 GHz are shown in Figs. 4(a)–4(c), respectively. As

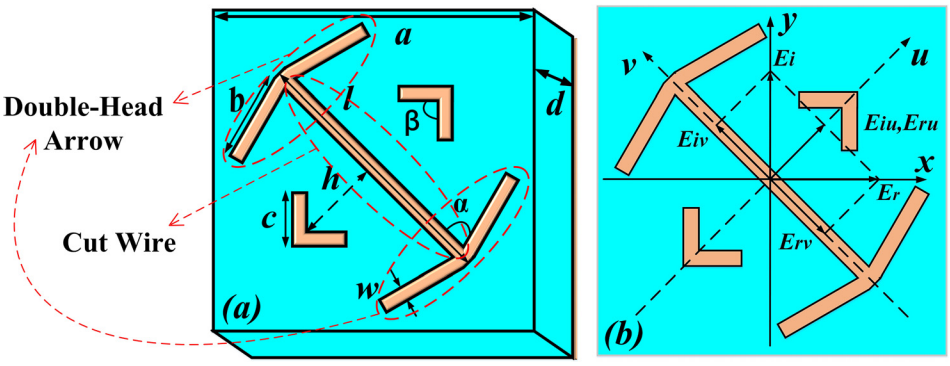

FIG. 1. (a) Front view of the metasurface unit cell. (b) Intuitive scheme of *y*- to *x*-polarization conversion of the metasurface. The *z*-axis is orthogonal to the *x*- and *y*-axes.

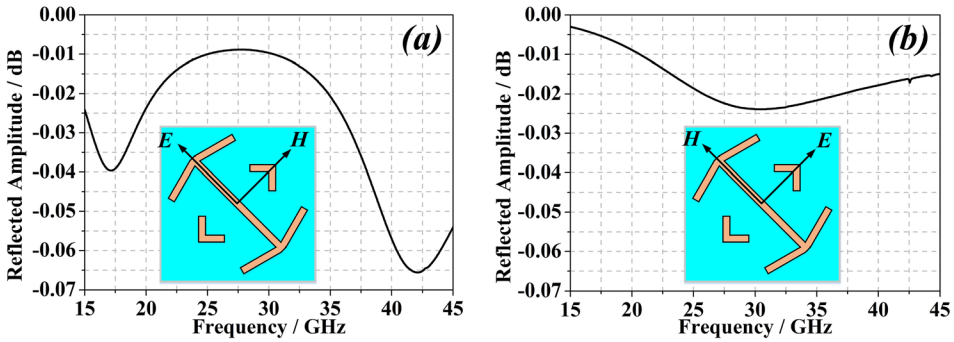

FIG. 2. The three eigen-modes of the unit cell under normal incidence: (a) *v*-polarized and (b) *u*-polarized.

shown in Figs. 4(a) and 4(c), the entire structure can be seen as an evolvement from cut-wire resonator, and hence, it functions as an extended cut wire resonator (extended by the presence of the head-arrows). Since the electric and magnetic resonances are generated by symmetric and anti-symmetric couplings of the currents on the extended cut wire resonator and metallic ground sheet, respectively, the resonance at 16.38 GHz is a magnetic resonance and the resonance at 42.03 GHz is an electric resonance (the electric and magnetic resonances are generated by parallel and anti-parallel surface currents induced along the entire structure and the metallic ground sheet, respectively). For *u*-polarization, it can be seen that an anti-symmetric mode is generated in the double-head arrow [Fig. 4(b)], and surface currents in the structure are anti-parallel to surface currents in the metallic ground sheet, leading to a magnetic resonance.

III. EXPERIMENTS

To verify the ultra-wideband polarization conversion capability of the proposed metasurface, full-wave simulations are performed in *CST Microwave Studio* with periodic boundary conditions in *x*- and *y*-directions and open additional space conditions along the $+z$ direction. Figure 5 shows the simulated co- and cross-polarization reflection and polarization conversion ratio (PCR). The cross-polarization reflection coefficients r_{yx} and r_{xy} are roughly 1 (0 dB) in a very wide frequency band, which means that polarization conversion can be achieved under both *x*- and *y*-polarized waves at normal incidence. This ultra-wideband polarization conversion property is the consequence of the three resonance frequencies at 19.59 GHz, 24.96 GHz, and 38.25 GHz, where the polarization conversion efficiency is nearly 100%, as shown in Fig. 5(b).

Moreover, we discuss the effect of the angle α and the cut-wire length l [see Fig. 1(a)] on the polarization conversion. The co- and cross-polarized reflection coefficients for different angles are shown in Figs. 6(a) and 6(b). When α is lower than 70°, the bandwidth decreases sharply. Similar effects, i.e., bandwidth reduction and conversion efficiency degradation, occur when l shortens (not shown).

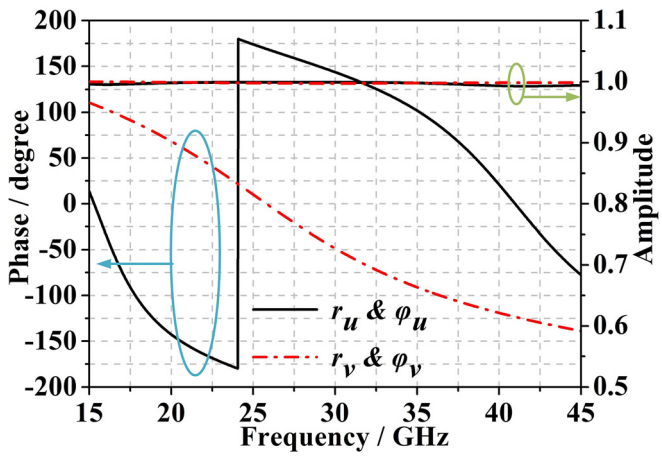

FIG. 3. Reflection amplitudes and phases in simulation for incident electromagnetic waves (EMWs) polarized with the electric field along *v*- and *u*-axes.

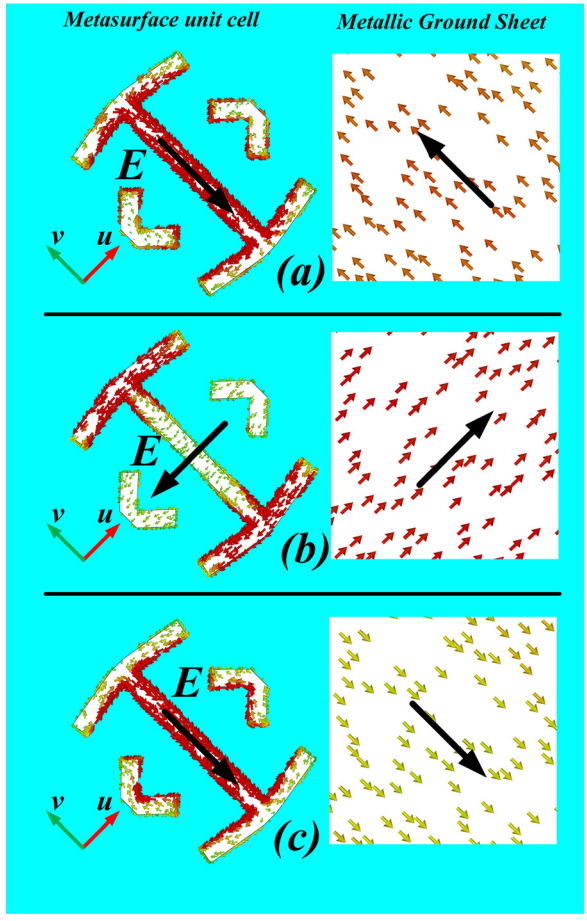

FIG. 4. Surface current distributions on the metallic parts of the metasurface unit cell and metallic ground sheet at three resonance frequencies: (a) 16.38 GHz, (b) 29.57 GHz, and (c) 42.03 GHz. The black big arrows indicate the main direction of current flow.

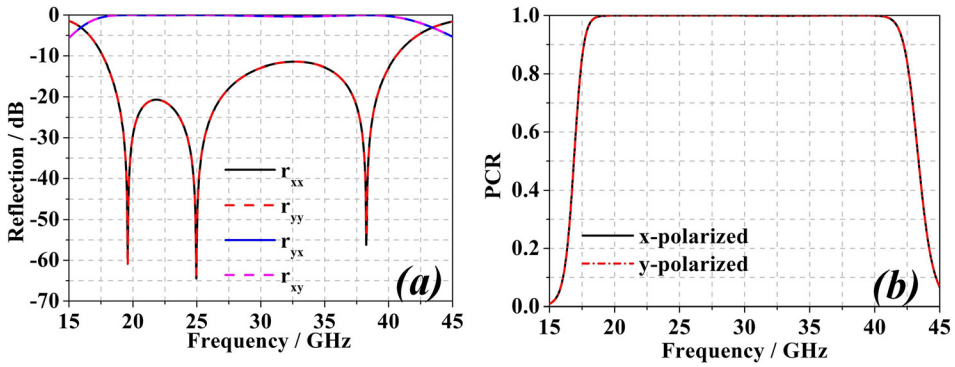

FIG. 5. Simulated co- and cross-polarization reflection coefficients (a) and polarization conversion ratio (b) of the designed polarization converter.

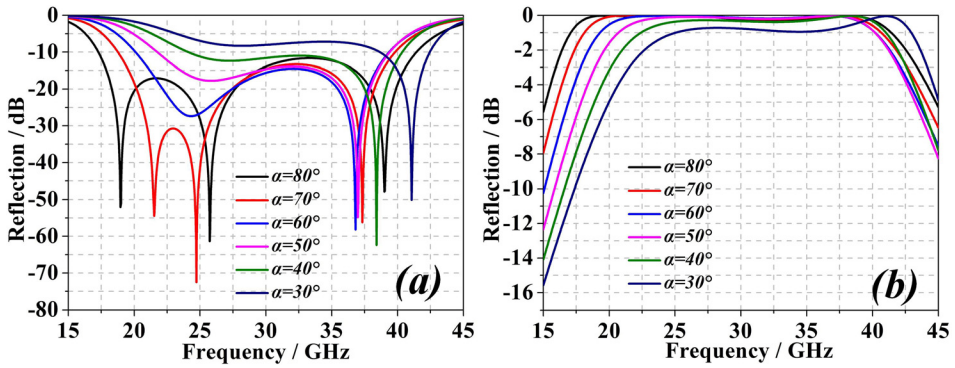

FIG. 6. Simulated reflection coefficients with α varying from 80° to 30°: (a) co-polarized and (b) cross-polarized.

It is also important to investigate the polarization conversion efficiency and bandwidth of our proposed metasurface for PWs with oblique incidence. The incident PW is considered to be polarized along the x-axis. The simulated PCR for different incident angles θ is depicted in Fig. 7. The incidence angle has no significant influence on polarization conversion bandwidth and efficiency, despite the fact that when θ is varied from 10° to 50° the number of resonances in co-polarized reflection coefficients reduces from three to two (not shown).

Figure 8(a) depicts the fabricated metasurface (with dimensions 300 mm × 300 mm). The experimental setup is illustrated in Fig. 8(b), in which one horn antenna is used as the source (transmitting antenna), and the other one is the receiving antenna. Both horn antennas are identical and they are connected to the vector network analyzer (VNA) *Agilent E8364B*. We first placed the antennas with the same polarization (horizontal or vertical) in order to measure the co-polarization reflection coefficients r_{xx} and r_{yy}, and then we rotated the receiver antenna in order to detect the cross-polarization reflection coefficient r_{yx} and r_{xy}. In both cases, r_{xx} (or r_{yy}) and r_{xy} (or r_{yx}) are given by the measured S_{21} parameter, or transmission coefficient between the input and output ports of the VNA, where the transmitting and receiver antennas are connected, respectively. However, the co- and cross-polarized reflection coefficients are actually given by the measured value of S_{21} referred to the value of S_{21} inferred from an ordinary metal surface with the same size, in order to compensate for the loss in the microwave link between the transmitting and receiving antennas. Note that we use F4B as the dielectric, and the losses increase as the frequency increases. However, we can still clearly observe three resonances at 19.68 GHz, 24.33 GHz, and 37.89 GHz in Fig. 9(a). Figure 9(b) shows the measured PCR of the metasurface, which indicates that the polarization conversion metasurface has an ultra-wideband characteristic. In addition, the polarization conversion properties of the metasurface under oblique incidences are evaluated by changing the incident angle θ from 10° to 50° as shown in Fig. 10. The experimental results are in good agreement with the simulations in spite of some interfering effects caused by measurement setup cables and connectors, as well as tolerances in material parameters and dimensions.

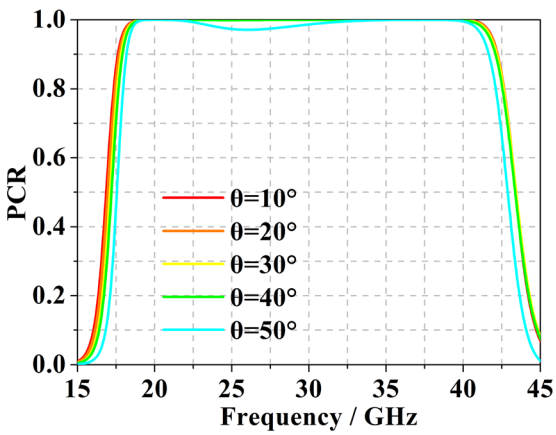

FIG. 7. Simulated PCR of the designed polarization converter under oblique incidence of EM waves with θ from 10° to 50°.

A comparison between the proposed converter and other polarization converters reported in Refs. 27 and 31 is shown in Table I. The comparison shows that the proposed converter is ultra-thin and has an ultra-wide frequency band in which PCR is greater than 90%, implying good performance. In Table I, *BW* means the operating absolute bandwidth (PCR > 90%) of the metasurface, and *BW* % means the relative bandwidth (PCR > 90%) of the metasurface. The

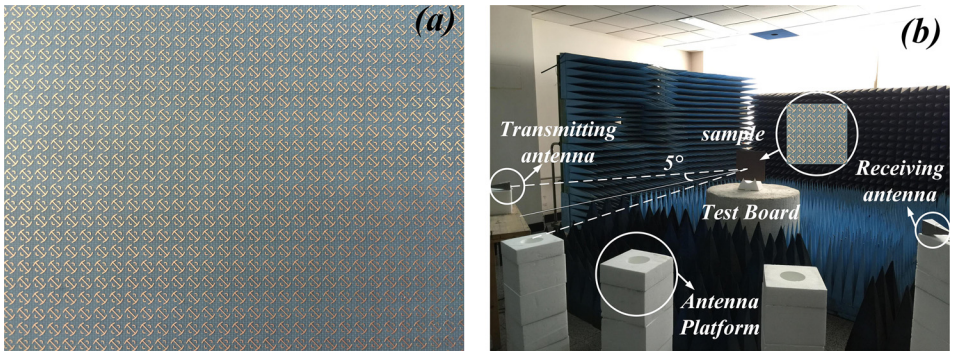

FIG. 8. (a) Fabricated metasurface and (b) experimental setup.

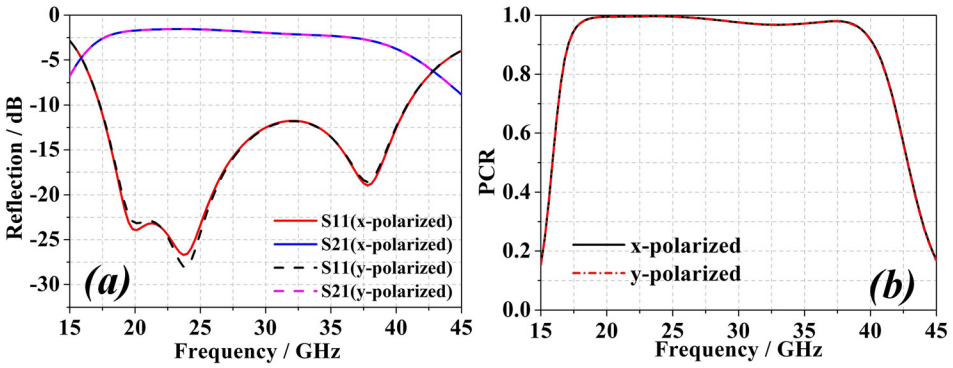

FIG. 9. (a) Measured co- and cross-polarization reflections of the polarization converter under normal incidence. (b) Measured PCR.

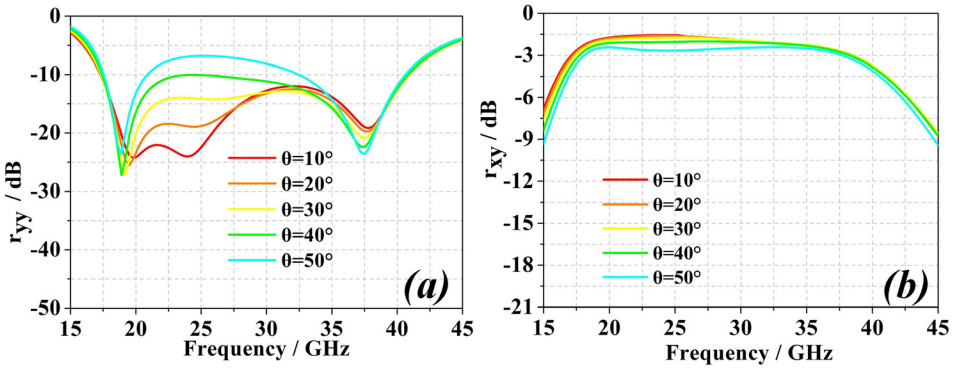

FIG. 10. Measured co- and cross-polarization reflection with θ varying from 10° to 50°: (a) r_{yy} and (b) r_{xy}.

parameters d and p are the dielectric substrate thickness of the metasurface and unit cell periodicity of the polarization conversion metasurface, respectively.

IV. CONCLUSION

In this work, a metasurface for ultra-wideband polarization conversion has been designed, fabricated, and verified through experiments. Due to the presence of three resonances, cross-polarization reflection bandwidth has been expanded significantly. To verify the excellent polarization conversion performance of the proposed metasurface, we have fabricated a sample polarization converter. Simulation and measurement results have shown that the proposed metasurface can convert linear polarized EM waves into cross-polarized waves with PCR higher than 90% from 17.3 GHz to 42.2 GHz. The physical mechanism behind the proposed metasurface has been investigated in detail through simulations. Additionally, we have also investigated the polarization conversion efficiency and bandwidth under oblique incidence PWs. The bandwidth and efficiency of the polarization conversion metasurface are immune to the incident angle from 0° to 50°, exhibiting a wide angle characteristic.

TABLE I. Comparison with other wideband polarization conversion metasurfaces.

	BW (GHz)	*BW* %	*d* (mm)	*p* (mm)
Reference 31	10.6–17.5	49	3	10
Reference 27	12.4–27.96	77	1.6	6.4
Present study	17.3–42.2	83	1.5	3

ACKNOWLEDGMENTS

The authors are grateful to the National Natural Science Foundation of China (61501227 and 61071019), Postdoctoral Science Foundation of China (2015M581789), Jiangsu Innovation Program for Graduate Education (KYLX16-0370), Fundamental Research Funds for the Central Universities (NJ20160011), MINECO-Spain (TEC2013-40600-R, TEC2016-75650-R), and Generalitat de Catalunya (2014SGR-157) and FEDER funds.

[1]N. K. Grady, J. E. Heyes, D. R. Chowdhury, Y. Zeng, M. T. Reiten, A. K. Azad, A. J. Taylor, D. A. Dalvit, and H.-T. Chen, Science **340**, 1304 (2013).
[2]D. Schurig, J. J. Mock, B. J. Justice, S. A. Cummer, J. B. Pendry, A. F. Starr, and D. R. Smith, Science **314**, 977 (2006).
[3]D. R. Smith, W. Padilla, D. Vier, S. Nemat-Nasser, and S. Schultz, Phys. Rev. Lett. **84**, 4184 (2000).
[4]C. Pfeiffer and A. Grbic, Appl. Phys. Lett. **102**, 23 (2013).
[5]T. Meissner and F. J. Wentz, IEEE Trans. Geosci. Remote Sens. **44**, 506 (2006).
[6]S. Sun, Q. He, S. Xiao, Q. Xu, X. Li, and L. Zhou, Nat. Mater. **11**, 426 (2012).
[7]Y. R. Padooru, A. B. Yakovlev, P. Y. Chen, and A. Alu, J. Appl. Phys. **112**, 104902 (2012).
[8]M. B. Pu, P. Chen, C. T. Wang, Y. Q. Wang, Z. Y. Zhao, C. G. Hu, C. Huang, and X. G. Luo, AIP Adv. **3**, 052136 (2013).
[9]Z. Li, L. Huang, K. Lu, Y. Sun, and L. Min, Appl. Phys. Express **7**, 112001 (2014).
[10]Z. Li, E. Palacios, S. Butun, and K. Aydin, Nano Lett. **15**, 1615 (2015).
[11]H. F. Ma, G. Z. Wang, W. X. Jiang, and T. J. Cui, Sci. Rep. **4**, 6337 (2014).
[12]N. F. Yu, F. Aieta, P. Genevet, M. A. Kats, Z. Gaburro, and F. Capasso, Nano Lett. **12**, 638 (2012).
[13]Y. Zhao and A. Alù, Phys. Rev. B **84**, 205428 (2011).
[14]J. G. Caputo, I. Gabitov, and A. I. Maimistov, Phys. Rev. B **11**, 91 (2015).
[15]L. Zhang, P. Zhou, H. Lu, L. Zhang, J. Xie, and L. Deng, Opt. Mater. Express **6**, 1393–1404 (2016).
[16]H. Chen, J. Wang, H. Ma, S. Qu, Z. Xu, A. Zhang, M. Yan, and Y. Li, J. Appl. Phys. **115**, 154504 (2014).
[17]S. L. Sun, Q. He, S. Y. Xiao, Q. Xu, X. Li, and L. Zhou, Nature Mater **11**, 426 (2012).
[18]Y. Cheng, Y. Nie, X. Wang, and R. Gong, Appl. Phys. A Mater. Sci. Process **111**, 209–215 (2013).
[19]H. Shi, A. Zhang, S. Zheng, J. Li, and Y. Jiang, Appl. Phys. Lett. **104**, 034102 (2014).
[20]Q. Lévesque, M. Makhsiyan, P. Bouchon, F. Pardo, J. Jaeck, N. Bardou, C. Dupuis, R. Haïdar, and J.-L. Pelouard, Appl. Phys. Lett. **104**, 111105 (2014).
[21]Z. Wei, Y. Cao, Y. Fan, X. Yu, and H. Li, Appl. Phys. Lett. **99**, 221907 (2011).
[22]J. K. Gansel, M. Thiel, M. S. Rill, M. Decker, K. Bade, V. Saile, G. von Freymann, S. Linden, and M. Wegener, Science **325**, 1513 (2009).
[23]J. M. Hao, Y. Yuan, L. X. Ran, T. Jiang, J. A. Kong, C. T. Chan, and L. Zhou, Phys. Rev. Lett. **99**, 063908 (2007).
[24]J. M. Hao, Q. J. Ren, Z. H. An, X. Q. Huang, Z. H. Chen, M. Qiu, and L. Zhou, Phys. Rev. A **80**, 023807 (2009).
[25]N. F. Yu, P. Genevet, M. A. Kats, F. Aieta, J. P. Tetienne, F. Capasso, and Z. Gaburro, Science **334**, 333 (2011).
[26]H. Chen, J. Wang, H. Ma, S. Qu, Z. Xu, A. Zhang, M. Yan, and Y. Li, J. Appl. Phys. **115**, 154504 (2014).
[27]X. Gao, X. Han, W. P. Cao, H. O. Li, H. F. Ma, and T. J. Cui, IEEE Trans. Antennas Propag. **63**, 3522 (2015).
[28]H. T. Chen, J. F. Zhou, J. F. O'Hara, F. Chen, A. K. Azad, and A. J. Taylor, Phys. Rev. Lett. **105**, 073901 (2010).
[29]H. T. Chen, Opt. Express **20**, 7165–7172 (2012).
[30]C. Chen, Z. Li, L. L. Liu, J. Xu, P. P. Ning, B. Z. Xu, X. L. Chen, and C. Q. Gu, Prog. Electromagn. Res. **154**, 79–85 (2015).
[31]H. Y. Chen, H. Ma, S. B. Qu, J. F. Wang, Y. F. Li, H. Y. Yuan, and Z. Xu, in *Proceedings of the IEEE Asia-Pacific Conference on Antennas and Propagation (APCAP)*, 2014, pp. 1009–1011.